ARTICLE

Plasmonic Control of the Shape of the Raman Spectrum of a Single Molecule in a Silver Nanoparticle Dimer

T. Dadosh,[†,‡] J. Sperling,[‡] G. W. Bryant,[§] R. Breslow,[∥] T. Shegai,[⊥] M. Dyshel,[†] G. Haran,[⊥,*] and I. Bar-Joseph[†,*]

[†]Department of Condensed Matter Physics, Weizmann Institute of Science, Rehovot, Israel, [‡]Department of Organic Chemistry, Weizmann Institute of Science, Rehovot, Israel, [§]National Institute of Standards and Technology, Gaithersburg, Maryland 20899, [∥]Department of Chemistry, Columbia University, New York, New York 10027, and [⊥]Department of Chemical Physics, Weizmann Institute of Science, Rehovot, Israel

ABSTRACT We study surface-enhanced Raman scattering (SERS) of individual organic molecules embedded in dimers of two metal nanoparticles. The good control of the dimer preparation process, based on the usage of bifunctional molecules, enables us to study quantitatively the effect of the nanoparticle size on the SERS intensity and spectrum at the single molecule level. We find that as the nanoparticle size increases the total Raman intensity increases and the lower energy Raman modes become dominant. We perform an electromagnetic calculation of the Raman enhancement and show that this behavior can be understood in terms of the overlap between the plasmonic modes of the dimer structure and the Raman spectrum. As the nanoparticle size increases, the plasmonic dipolar mode shifts to longer wavelength and thereby its overlap with the Raman spectrum changes. This suggests that the dimer structure can provide an external control of the emission properties of a single molecule. Indeed, clear and systematic differences are observed between Raman spectra of individual molecules adsorbed on small *versus* large particles.

KEYWORDS: surface plasmon · SERS · surface-enhanced Raman scattering · single molecule · dimers · silver colloids · nanoparticles

Raman spectroscopy is known to be a powerful tool that provides a spectral fingerprint of molecules. Its implementation to the study of single molecules is, however, difficult due to the small cross section of the process. Surface-enhanced Raman scattering (SERS), however, may amplify the Raman signal by more than 10 orders of magnitude and, hence, is considered to be an attractive methodology for single molecule spectroscopy.[1−4] SERS occurs when a molecule is adsorbed on a metal surface possessing curvature with a characteristic length of 10−100 nm and has been realized on metal gratings,[5] lithographically defined spheroid assemblies,[6] and nanometer-sized metallic colloids.[7] The understanding of the mechanism responsible for the gigantic amplification seen in SERS has been a subject for active research for the past three decades.[8] The dominant mechanism is believed to be the interaction between the electromagnetic radiation and the mobile surface charges in the metal. The surface plasmons which are excited by this interaction give rise to a strong electric field near the metal surface, which in turn enhances the Raman scattering from molecules located in this region.[9] The chemical enhancement, which occurs due to the interaction between the metallic and molecular electronic states, is believed to play a less important role.[10]

Recent studies suggest that the SERS enhancement is substantially increased when a molecule resides in the junction between two nanoparticles (NPs).[11] As two NPs approach each other, the near-field of one particle interacts with the electrons in the adjacent particle, coupling the plasmon oscillations together. This coupling yields a significantly stronger near-field in the junction compared to that which exists around a single particle.[12] Experimental indications for the importance of this coupling were provided by several works, implementing different experimental techniques.[3,11,13−15]

In this paper, we present SERS measurements utilizing *pre-prepared* junctions in dimeric NP structures,[16] consisting of silver NPs of a relatively narrow size distribution, and a short organic molecule that bridges them. This enables us to conduct a controlled and quantitative study of the SERS enhancement at the single molecule level and, in particular, to study the dependence of SERS intensity and spectrum on NP size. We find that as the NP size is increased the total SERS intensity increases and the spectrum changes such that the lower energy Raman modes become dominant. In that sense, the NP size can be used to shape the Raman spectrum in a manner similar to the way the distance between NPs was recently demonstrated to affect the molecular fluo-

*Address correspondence to israel.bar-joseph@weizmann.ac.il, gilad.haran@weizmann.ac.il.

Received for review April 28, 2009 and accepted June 10, 2009.

Published online June 17, 2009. 10.1021/nn900422w CCC: $40.75

rescence spectrum.[17] To explain this behavior, we perform electromagnetic calculation of the Raman enhancement in these structures. We find that the plasmon absorption spectrum of the dimer exhibits a strong red shift as the NP size increases and thereby increases the overlap between the plasmon and Raman spectra. Since the SERS enhancement strongly depends on this overlap, we obtain an increased enhancement with NP size; the low energy Raman modes, which are closer to the plasmon modes, are amplified more strongly.

RESULTS AND DISCUSSION

Our ability to form metal−molecule structures allowed us to establish quantitatively the relation between the SERS enhancement and the formation of conjugated structures such as NP dimers. The first step was to form dimers, in which a *single* organic molecule binds to two NPs.[16] In selecting the appropriate molecules for SERS measurement, we had to account for two requirements: First, the molecule should have chemical groups on both ends with a high affinity to silver, such that a stable dimeric structure could be formed, with a fixed interparticle distance. Second, the molecular absorption should peak near the silver NP plasmon resonance. Two molecules that satisfy these requirements were used: Rhodamine123 (Rh123), which contains two amine groups at the xanthene ring (Figure 1c), with peak absorption at 515 nm, and the polythiophene T4, which contains four thiophene rings and thiophenol groups at its two ends (Figure 1d),[18] with peak absorption at 420 nm. The procedure for the formation of dimer structures with T4 and Rh123 was similar to that described in our early work[16] (see details in the Materials and Methods section). We prepared two dimer solutions of T4-bridged Ag NPs and Rh123-bridged Ag NPs which contained about 30% NP dimers and 70% single NPs (with a small fraction of larger cluster of particles: trimers, tetramers, *etc.*). In the first set of experiments, we used silver NPs that were prepared following the Lee−Meisel protocol.[19] We adsorbed the particles on a patterned glass substrate prepared using optical lithography with a labeled grid of 10 μm × 10 μm squares and measured the Raman signal. To improve the adsorption uniformity, the cover glass was treated with polylysine (1 mg/mL) prior to the adsorption. The samples were excited using a frequency-doubled Nd^{2+}-YVO4 laser at 532 nm for the Rh123 measurements and an argon ion laser at 488 nm for the T4 measurements. We first recorded an image of an illuminated square with the grating at zeroth order, effectively

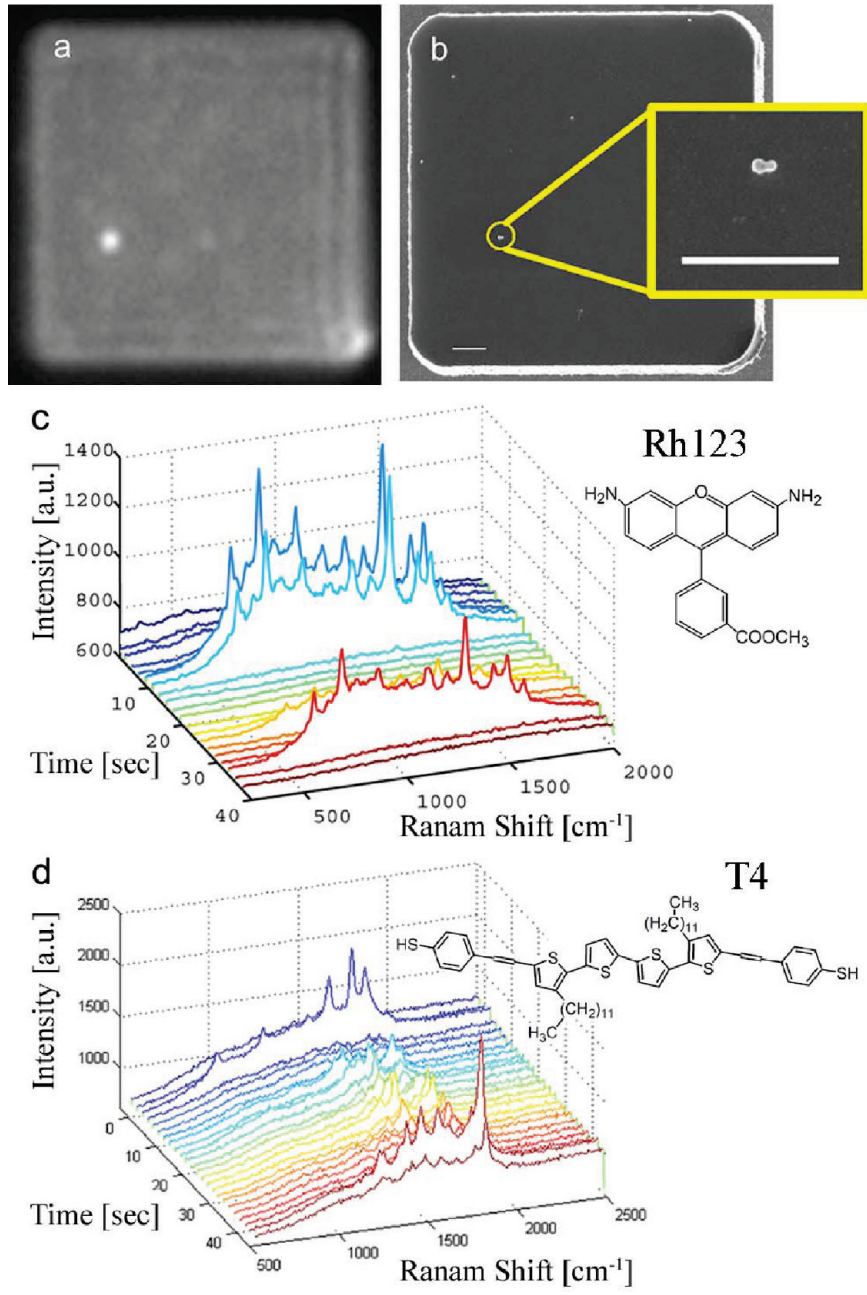

Figure 1. (a) Image of a 10 μm × 10 μm square that contains a single Raman-active dimer (the bright spot). (b) SEM image of the same square. At the location of the Raman spot, a dimer is clearly observed (inset). All other objects in this square are single nanoparticles. (c,d) Time series of SERS spectra of Rh123 and T4, respectively, showing the characteristic single molecule blinking. Insets: Chemical structure of Rhodamine 123 and T4.

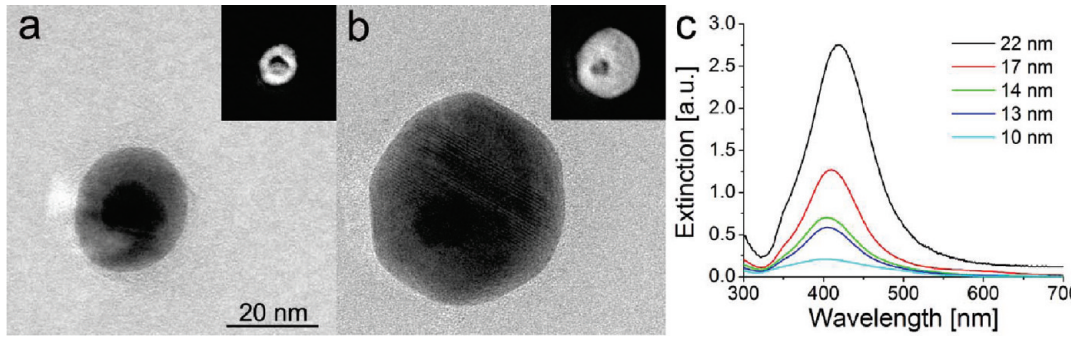

Figure 2. (a,b) TEM images of NPs with a gold core of a 6.3 nm radius and silver shells of 12 and 22 nm radii, respectively. Insets: silver element mapping of the NPs by using energy-filtered TEM, in the range of 377−407 eV. The bright areas are attributed to silver in the shell region. (c) Extinction spectra of solutions of core−shell NPs with a 6.3 nm gold core radius and different shell radii (normalized to NP concentration of 0.15 nM).

acting as a mirror. Raman-active NPs appeared in this image as bright spots within the illuminated square (Figure 1a). We then rotated the grating to its first order position and collected the Raman spectrum from each hot spot. The spectrum exhibited the characteristic blinking behavior known for single molecules (Figure 1c,d).

To identify the nanostructure that was responsible for the Raman signal, we imaged the sample in SEM, where a detailed picture of the adsorbed NPs at each square could be obtained (Figure 1b). We have analyzed in this manner more than 60 high intensity spots of T4− and Rh123−NP dimers and found that in 94% of the cases the origin of the bright spot was a dimeric structure (see example in the inset of Figure 1b). The remaining 6% was due to larger clusters of particles. Single NPs did not give rise to a detectable SERS signal. With the signal-to-noise ratio of our experiment, we can estimate that the SERS cross section from single NPs is at least 100 times smaller than that of dimers. This finding clearly underlines the importance of such conjugates in SERS enhancement.

The small detuning of the 532 nm line with respect to the peak absorption of Rh123, which implies that the Raman signal was also enhanced by the molecular resonance, enabled us to conduct the measurements of this molecule at much smaller power densities than those required for T4 (the typical excitation intensity for Rh123 was 30−200 W/cm^2; T4 was excited with a typical intensity of 600 W/cm^2), and the recorded spectra were therefore much more stable, allowing reliable spectral measurements. Most of the results presented in this paper are therefore for Rh123.

It is well-known that SERS enhancement in silver structures is larger than in structures made of other coinage metals.[8] However, the high reactivity of silver compounds makes it difficult to produce NPs with a well-controlled size. Indeed, the Lee−Meisel silver NPs have a very broad size distribution. To obtain a preparation with a narrow size distribution, we synthesized NPs that consist of gold cores and a silver shell (Figure 2a,b). The colloids prepared in this way were characterized by a standard deviation of 15% or less of their mean diameter (measured using TEM). We found that the maximum absorption of the gold NP solution, prior to coverage with silver, is at 520 nm, and it is blue-shifted by about 100 nm toward the typical plasmon resonance wavelength of silver during the silver shell growth. The resulting plasmon spectra for NPs with a

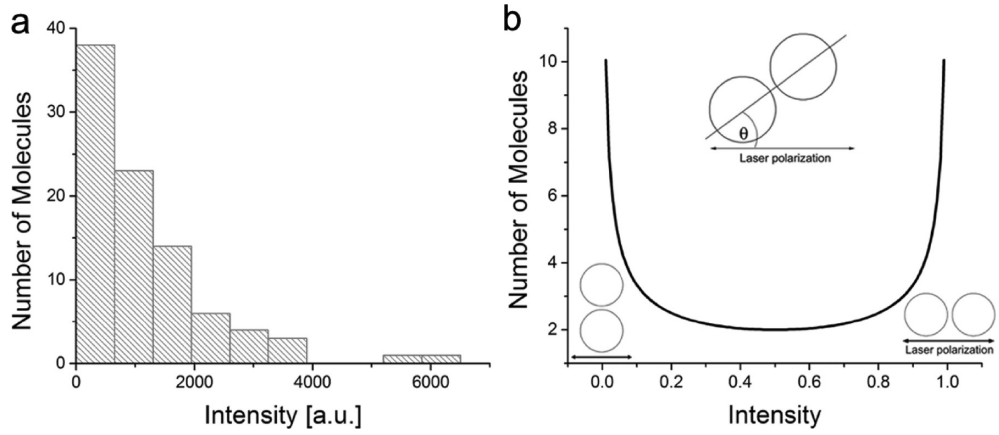

Figure 3. (a) Histogram of the SERS intensity measured for 17 nm nanoparticles. (b) Theoretical SERS intensity distribution, eq 1, assuming that the intensity is related to the angle θ, and that it is high for the parallel configuration and low for the perpendicular configuration.

core radius of 6.3 nm and variable sizes of the shell are shown in Figure 2c.

To characterize the Raman intensity emitted from molecules within NP dimers of various sizes, we integrated the measured spectrum over frequency. We observed a large variability in the integrated intensities of different molecules, spanning more than an order of magnitude. To explain this variability, one should take into account the relative angle θ between the (linear) laser polarization and the dimer orientation.[20] When it is assumed that the NP dimers are distributed on the substrate such that they have equal probability for all possible angles, the expected distribution of the measured SERS intensities is given by

$$\left|\frac{d\theta}{dI}\right| \sim \frac{1}{\sqrt{I/I_{max} - (I/I_{max})^2}} \quad (1)$$

This implies that the intensity distribution should have two maxima, at low and high intensities, and the probability to get intermediate intensities should be relatively low (Figure 3a). Indeed, the intensity histogram of the measured dimers exhibits such a double-branch behavior: a strong decaying branch at low intensities, and a second branch at the highest intensities, which is significantly weaker. We believe that the reason for the reduced probability to observe high intensity SERS is the fast disappearance of these signals due to photodamage of the molecules. Indeed, we observed that the brighter hot spots decayed very fast, to the extent that we could not accurately record their intensity.

The understanding of the SERS intensity distribution enables us to determine the characteristic average SERS intensity for each NP size from the measured data. Intensity values were obtained from integrated spectra of 20 to 90 hot spots for each type of NP dimers. From the low intensity branch of the histogram obtained from the data of each dimer type, we extracted the average intensity. Figure 4a,b shows the average SERS intensity as a function of the NP radius for two sets of Rh123−NP dimers (with NP gold-core radius of 6.3 and 9.2 nm, respectively). It is seen that these two sets show the same trend: the SERS signal increases as the NP size grows. The observed behavior clearly shows that the SERS enhancement is related to plasmon effects in the NPs which are adjacent to the molecule. Yet it is not obvious why this enhancement should depend on the NP size in the particular manner observed in the experiment. We therefore conducted an electromagnetic calculation of the near-field in the junction of a dimer using the boundary element method[21] and studied its dependence on NP size, excitation wavelength, and the spacing between the NPs. Retardation effects were explicitly included. In the following, we limit the discussion to the case where the separation between the two NPs is 1 nm, which is approximately the length of the Rh123 molecule, which bridges the gap between NPs.

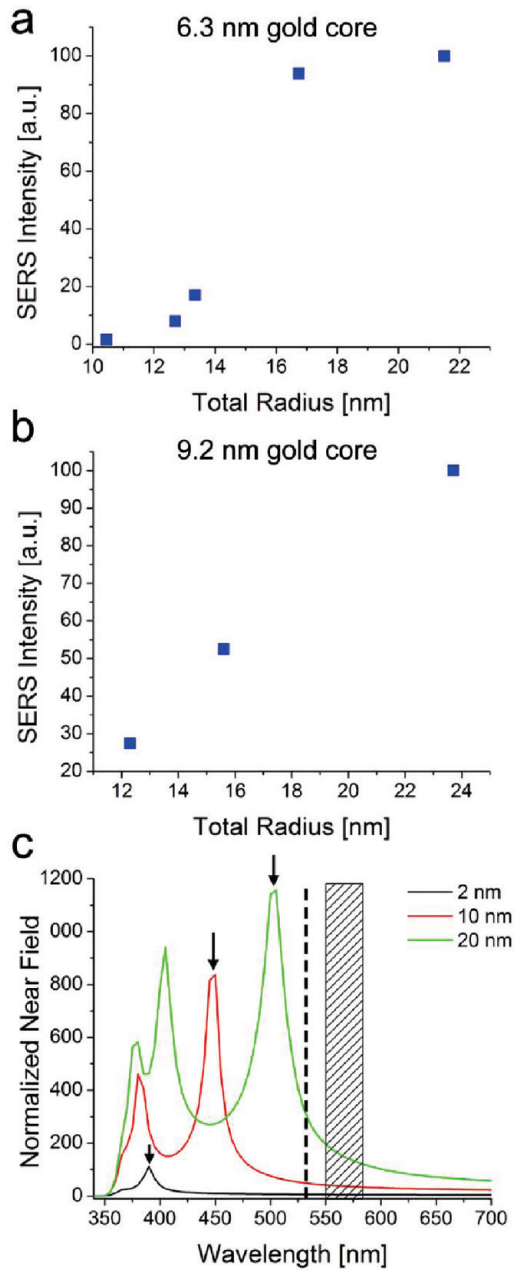

Figure 4. (a,b) Measured SERS intensity as a function of the overall NP radius for two gold core radii. (c) Calculated normalized near-field at the junction of a dimer (with a gap of 1 nm) for Ag dimers with 2, 10, and 20 nm NPs radii. The dashed line indicates the 532 nm excitation wavelength. It is seen that as the NP gets larger the dipole mode (marked by an arrow) moves to longer wavelength and higher multipole peaks appear at shorter wavelengths. The dashed area represents the range of the Raman spectrum of Rh123.

Figure 4c shows the near-field at midgap as a function of wavelength for various sizes of NPs (the calculations are for a plane wave polarized parallel to the principal axis of the dimer). It is seen that dimers which consist of small NPs (radius 2 nm) exhibit a single resonance. For these NP sizes, the quasi-static approximation is valid, and one obtains a single dipolar plasmon. As the NPs get larger, this simple spectral behavior changes into a more complex one: the dipole peak red shifts to longer

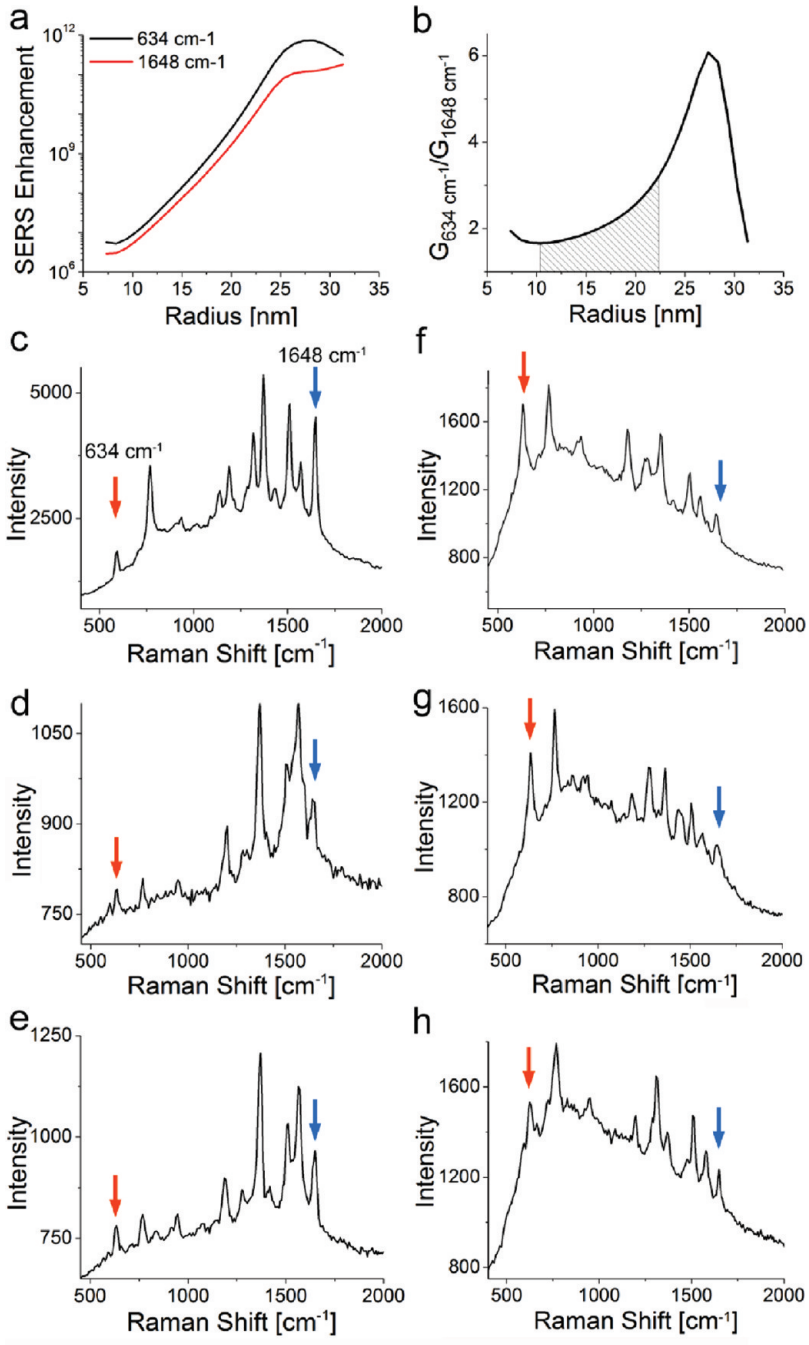

Figure 5. (a) Calculated SERS enhancement at the junction of two core−shell NPs as a function of NP radius (with a constant Au core of a 6.3 nm radius) for $\lambda_{excitation}$ = 532 nm and $\lambda_{emission}$ = 550 and 582 nm (which correspond to Raman shifts of 634 and 1648 cm^{-1}, respectively). The separation between the two NPs is 1 nm, and the environment has an effective dielectric constant of 1.5. (b) Enhancement of the 634 cm^{-1} Raman mode relative to that of the 1648 cm^{-1} mode as a function of the NP radius. The dashed area is the one explored in our experiment. (c−e) SERS spectra of various Rh123 dimers of a 14 nm radius. (f−h) SERS spectra of various Rh123 dimers of 22 nm radius. The red and blue arrows identify the 634 and 1648 cm^{-1} Raman modes, respectively.

wavelengths, and higher multipole peaks appear at short wavelengths. These changes are attributed mainly to increased coupling between the NPs with increasing of their size.

The effect of this complex spectral behavior on the Raman enhancement can be assessed by considering the fact that the overall SERS enhancement, $G(\omega) = |E(\omega)|^2|E_{ex}|^2$, is a product of the enhanced near-fields at the midgap, $E(\omega)$ at the excitation frequency, and E_{ex} at the Stokes-shifted frequency. One can see in Figure 4c that, for small NPs, the first mode is at a shorter wavelength than the 532 nm excitation wavelength, and the overlap between the plasmon spectrum, the excitation laser, and Raman lines is very small. As the particle size increases, the dipole mode, marked by an arrow in Figure 4c, is shifted to longer wavelengths, and higher multipole peaks appear at shorter wavelength. As a result, the overlap of the plasmon spectrum with the excitation and emission wavelengths increases. Figure 5a shows the calculated size dependence of the enhancement at the lowest and highest Raman modes of Rh123 (634 and 1648 cm^{-1}) when excited at 532 nm. Note that molecular enhancement effects on the intensities of the two modes are not included in this calculation. These effects, however, remain constant as the sizes of the NPs change. It is seen that in the NP size range studied in our experiment (10−22 nm radii) the Raman spectrum gets stronger as the NP size increases, in a qualitative agreement with the observed behavior in Figure 4a,b. One should note, however, that this dependence does not persist for larger particle sizes, and a maximum is expected at a certain large NP size.

Interestingly, increasing the NP size is not expected to affect different Raman modes in the same manner. Figure 5b compares the increase in intensity of the lowest (634 cm^{-1}) and highest (1648^{-1}) Raman modes in the spectrum of Rh123 as the NP size increases. It is seen that the lowest mode experiences a larger intensity increase (by a factor of 2−3 at this NP size range) compared to the highest mode. This effect is indeed seen experimentally. Figure 5c−h shows a comparison between the Raman spectra of dimers with 14 nm NPs and dimers with 22 nm NPs. It can be clearly seen that spectra of the larger NPs are tilted such that the low energy lines are stronger: the intensity of the 634 cm^{-1} mode is increased by a factor of 1.6 relative to the 1648 cm^{-1} mode as the size of the NP increased from 14 to 22 nm, in excellent agreement with the predicted behavior (Figure 5b). The underlying physics can be easily understood by examining Figure 4c: the low

energy Raman modes, which are closer in energy to the laser line, are also closer to the plasmon dipolar peak. As the NP size is increased, the difference in plasmonic enhancement between the low and high energy parts of the Raman spectrum increases and the spectrum is tilted.

This behavior is closely related to the recent report on shaping the emission spectra of fluorescent molecules with plasmonic nanoresonators.[17] In that work, the control parameter was the distance between the NPs, while in our work, it is the NP size. In both cases, the change of the control parameter caused the plasmonic spectrum to red shift and thereby affected the overlap with the Raman or fluorescence spectrum. It appears, however, that the technique demonstrated in our work has an inherent advantage, as it allows the manipulation of the spectrum at the single molecule level, where the distance between the NPs is fixed by the molecule's length.

As a final note, we wish to comment that we have previously shown that the dimer structure is also a convenient system for electrically contacting a single organic molecule.[16] The fact that this same structure gives rise to a pronounced Raman signal may pave the way for simultaneous measurements of the transport and Raman properties and thereby give access into the coupling between electrical transport and inelastic scattering at the molecule.[22]

MATERIALS AND METHODS

Silver NPs were prepared following the Lee−Meisel protocol.[19] The synthesis process of core−shell of gold−silver NPs started with the preparation of monodispersed gold seeds of a radius of 6.3 or 9.2 nm (characterization of the nanoparticles was carried out using TEM; the typical standard deviation is below 10%).[23] These gold seeds were added to a 50 mL solution of $AgNO_3$ in double-distilled water (DDW) (concentrations are listed in Table 1), which was heated to 70 °C in a reflux setup. Then, 4 mL of 1% trisodium citrate was added. The solution changed its reddish color to yellow and was further boiled for 90 min. Colloids with a relatively narrow size distribution were obtained and characterized by a standard deviation of less than 15% of the diameter, as determined from TEM images.

The preparation of T4-bridged Ag NPs was carried out following the procedures in Dadosh *et al.*[16] T4 (inset Figure 1) was synthesized with thioester protecting groups at both ends.[18] Then, the protected T4 was dissolved in tetrahydrofuran (THF) at 1×10^{-6} M. Ammonium hydroxide (10 μL of 15 M) was added to 1 mL of the T4 solution, and the mixture was incubated for 60 min to cleave the thioester protecting groups. An equivalent amount of acetic acid (10 μL of 16 M) was added for neutralization; the unprotected T4 solution was diluted in DDW to 0.1 nM, and 100 μL was mixed immediately with 900 μL of the Ag colloid solution made up by mixing 390 μL of DDW, 10 μL of 100 mM NaCl, and 500 μL of 0.2 nM Ag NPs. The 1:10 ratio of bridging molecules to NPs was chosen to ensure the formation of single molecule bridges. The reaction mixture was incubated at 4 °C for 24 h, and the concentration of the bridged NPs was increased from 10 to 30% by mild centrifugation (determined by counting the NPs dimers in the solution deposited on a copper grid using TEM). We note that there was a large fraction of dimers which were formed due to salt aggregation and did not give rise to Raman signal. Rh123-bridged Ag NPs were prepared by using the same method. Rh123 was dissolved in ethanol at approximately 10^{-5}M (the concentration was determined by its absorption at 510 nm using its extinction of 85 000 M^{-1} cm^{-1}), diluted in DDW to 0.1 nM, and 100 μL was mixed with 900 μL of the Ag colloid solution made up by mixing 390 μL of DDW, 10 μL of 100 mM NaCl, and 500 μL of 0.2 nM Ag NPs. Incubation and concentration of the Rh123-bridged NPs were as described above.

To facilitate identifying nanoparticle structures that give rise to SERS hot spots, we prepared a substrate labeled with grid of 10 μm × 10 μm squares using optical lithography. Image reversal photoresist AZ5214E was used for patterning (spin coating 5000 rpm, 40 s, baked at 100 °C for 5.5 min) microcover glasses (Thomas) with the dimensions of 18 × 18 mm and 1.5 mm thickness. The glass and the electron-beam defined grid mask were aligned and exposed to 415 nm light at 15 mW for 5.5 s, then baked (1 min at 120 °C) and flood exposed for 1.5 min. The pattern was developed with developer AZ726 for 25 s, followed by thermal evaporation of a Ti (5 nm) adhesion layer and a 200 nm Au layer, and lifted off.

Samples for SERS measurements were prepared using the predefined substrate. The substrate was glued to a Teflon holder using nail polish. Polylysine (1 mg/mL) was adsorbed on the glass for 30 min, and the glass was then washed with DDW and blow-dried with air. The sample solution was drop-cast for about 10 min (while keeping it in dark), washed with DDW, and then blow-dried with air. After performing the SERS measurements, the sample was examined with SEM. The sample was coated before imaging in the SEM with a 2 nm layer of titanium to increase the quality of the SEM images by avoiding excessive charging by the electron beam.

TABLE 1. Reaction Conditions for Core−Shell Particle Synthesis and Sizes of Resulting Particles

$AgNO_3$ [mM]	Au core [nM]	Au core radius [nm]	colloid radius (core + shell) [nm]	standard deviation [%]
0.26	1.05	6.3	22	15
0.48	0.95	6.3	17	14
0.24	0.95	6.3	14	13
0.43	0.86	6.3	13	12
0.10	0.95	6.3	10	9
0.76	0.45	9.2	24	13
0.19	0.45	9.2	16	10
0.08	0.45	9.2	12	9

Acknowledgment. This work was supported by the Israel Ministry of Science and Technology, and the Israel Science foundation. The electron microscopy studies were conducted at the Irving and Cherna Moskowitz Center for Nano and Bio-Nano Imaging at the Weizmann Institute of Science. We wish to thank Dr. R. Popovich for assistance in obtaining the TEM images (Figure 2). We also acknowledge the help of Dr. P. Plochocka in the early stage of this project, and Dr. I. W. Tam in synthesizing the polythiophene molecules.

REFERENCES AND NOTES

1. Kneipp, K.; Wang, Y.; Kneipp, H.; Perelman, L. T.; Itzkan, I.; Dasari, R. R.; Feld, M. S. Single Molecule Detection Using Surface-Enhanced Raman Scattering (SERS). *Phys. Rev. Lett.* **1997**, *78*, 1667–1670.
2. Nie, S.; Emory, S. R. Probing Single Molecules and Single Nanoparticles by Surface-Enhanced Raman Scattering. *Science* **1997**, *275*, 1102–1106.
3. Xu, H. X.; Bjerneld, E. J.; Kall, M.; Borjesson, L. Spectroscopy of Single Hemoglobin Molecules by Surface Enhanced Raman Scattering. *Phys. Rev. Lett.* **1999**, *83*, 4357–4360.
4. Weiss, A.; Haran, G. Time-Dependent Single-Molecule Raman Scattering as a Probe of Surface Dynamics. *J. Phys. Chem. B* **2001**, *105*, 12348–12354.

5. Mattei, G.; Quagliano, L. G.; Pagannone, M. Surface-Enhanced Raman-Scattering (SERS) on Silver Surfaces Activated by a Simple Chemical Treatment. *Europhys. Lett.* **1990**, *11*, 373–378.
6. Jensen, T. R.; Malinsky, M. D.; Haynes, C. L.; van Duyne, R. P. Nanosphere Lithography: Tunable Localized Surface Plasmon Resonance Spectra of Silver Nanoparticles. *J. Phys. Chem. B* **2000**, *104*, 10549–10556.
7. Albano, E. V.; Daiser, S.; Ertl, G.; Miranda, R.; Wandelt, K.; Garcia, N. Nature of Surface-Enhanced-Raman-Scattering Active-Sites on Coldly Condensed Ag Films. *Phys. Rev. Lett.* **1983**, *51*, 2314–2317.
8. Moskovits, M. Surface-Enhanced Spectroscopy. *Rev. Mod. Phys.* **1985**, *57*, 783–826.
9. García-Vidal, F. J.; Pendry, J. B. Collective Theory for Surface Enhanced Raman Scattering. *Phys. Rev. Lett.* **1996**, *77*, 1163–1166.
10. Campion, A.; Ivanecky, J. E., III; Child, C. M.; Foster, M. On the Mechanism of Chemical Enhancement in Surface-Enhanced Raman Scattering. *J. Am. Chem. Soc.* **1995**, *117*, 11807–11808.
11. Michaels, A. M.; Jiang, J.; Brus, L. Ag Nanocrystal Junctions as the Site for Surface-Enhanced Raman Scattering of Single Rhodamine 6G Molecules. *J. Phys. Chem. B* **2000**, *104*, 11965–11971.
12. Xu, H. X.; Aizpurua, J.; Kall, M.; Apell, P. Electromagnetic Contributions to Single-Molecule Sensitivity in Surface-Enhanced Raman Scattering. *Phys. Rev. E* **2000**, *62*, 4318–4324.
13. Talley, C. E.; Jackson, J. B.; Oubre, C.; Grady, N. K.; Hollars, C. W.; Lane, S. M.; Huser, T. R.; Nordlander, P.; Halas, N. J. Surface-Enhanced Raman Scattering from Individual Au Nanoparticles and Nanoparticle Dimer Substrates. *Nano Lett.* **2005**, *5*, 1569–1574.
14. Suh, Y. D.; Schenter, G. K.; Zhu, L.; Lu, H. P. Probing Nanoscale Surface Enhanced Raman-Scattering Fluctuation Dynamics Using Correlated AFM and Confocal Ultramicroscopy. *Ultramicroscopy* **2003**, *97*, 89–102.
15. Khan, I.; Cunningham, D.; Lazar, S.; Graham, D.; Ewen Smith, W.; McComb, D. W. A TEM and Electron Energy Loss Spectroscopy (EELS) Investigation of Active and Inactive Silver Particles for Surface Enhanced Resonance Raman Spectroscopy (SERRS). *Faraday Discuss.* **2006**, *132*, 171–178.
16. Dadosh, T.; Gordin, Y.; Krahne, R.; Khivrich, I.; Mahalu, D.; Frydman, V.; Sperling, J.; Yacoby, A.; Bar-Joseph, I. Measurement of the Conductance of Single Conjugated Molecules. *Nature* **2005**, *436*, 677–680.
17. Ringler, M.; Schwemer, A.; Wunderlich, M.; Nichtl, A.; Kurzinger, K.; Klar, T. A.; Feldmann, J. Shaping Emission Spectra of Fluorescent Molecules with Single Plasmonic Nanoresonators. *Phys. Rev. Lett.* **2008**, *100*, 203002.
18. Tam, I. W.; Yan, J.; Breslow, R. An 11 nm Molecular Wire that Switches Electrochemically between an Insulating and a Fully Conjugated Conducting State. *Org. Lett.* **2006**, *8*, 183–185.
19. Lee, P. C.; Meisel, D. Adsorption and Surface-Enhanced Raman of Dyes on Silver and Gold Sols. *J. Phys. Chem.* **1982**, *86*, 3391–3395.
20. Le Ru, E. C.; Grand, J.; Félidj, N.; Aubard, J.; Lévi, G.; Hohenau, A.; Krenn, J. R.; Blackie, E.; Etchegoin, P. G. Experimental Verification of the SERS Electromagnetic Model beyond the $|E|^4$ Approximation: Polarization Effects. *J. Phys. Chem. C* **2008**, *112*, 8117–8121.
21. Aizpurua, J.; Bryant, G. W.; Richter, L. J.; Garcia de Abajo, F. J.; Kelley, B. K.; Mallouk, T. Optical Properties of Coupled Metallic Nanorods for Field-Enhanced Spectroscopy. *Phys. Rev. B* **2005**, *71*, 235420/1–235420/13.
22. Ward, D. R.; Halas, N. J.; Ciszek, J. W.; Tour, J. M.; Wu, Y.; Nordlander, P.; Natelson, D. Simultaneous Measurements of Electronic Conduction and Raman Response in Molecular Junctions. *Nano Lett.* **2008**, *8*, 919–924.
23. Slot, J. W.; Geuze, H. J. A New Method of Preparing Gold Probes for Multiple-Labeling Cytochemistry. *Eur. J. Cell Biol.* **1985**, *38*, 87–93.